

Disorders of the Nervous System

# Single Dose of Amphetamine Induces Delayed Subregional Attenuation of Cholinergic Interneuron Activity in the Striatum

 Samira Ztaou,<sup>1,2</sup>  Soo Jung Oh,<sup>1,2</sup> Sophia Tepler,<sup>1,2</sup> Sixtine Fleury,<sup>1,2</sup> Miriam Matamales,<sup>3</sup> Jesus Bertran-Gonzalez,<sup>3</sup> Nao Chuhma,<sup>1,2</sup> and  Stephen Rayport<sup>1,2</sup>

<https://doi.org/10.1523/ENEURO.0196-21.2021>

<sup>1</sup>Department of Molecular Therapeutics, New York State Psychiatric Institute, New York, NY 10032, <sup>2</sup>Department of Psychiatry, Columbia University, New York, NY 10032, and <sup>3</sup>Decision Neuroscience Laboratory, School of Psychology, University of New South Wales, Sydney, NSW 2052, Australia

## Abstract

Psychostimulants such as amphetamine (AMPH) target dopamine (DA) neuron synapses to engender drug-induced plasticity. While DA neurons modulate the activity of striatal (Str) cholinergic interneurons (ChIs) with regional heterogeneity, how AMPH affects ChI activity has not been elucidated. Here, we applied quantitative fluorescence imaging approaches to map the dose-dependent effects of a single dose of AMPH on ChI activity at 2.5 and 24 h after injection across the mouse Str using the activity-dependent marker phosphorylated ribosomal protein S6 (p-rpS6<sup>240/244</sup>). AMPH did not affect the distribution or morphology of ChIs in any Str subregion. While AMPH at either dose had no effect on ChI activity after 2.5 h, ChI activity was dose dependently reduced after 24 h specifically in the ventral Str/nucleus accumbens (NAc), a critical site of psychostimulant action. AMPH at either dose did not affect the spontaneous firing of ChIs. Altogether this work demonstrates that a single dose of AMPH has delayed regionally heterogeneous effects on ChI activity, which most likely involves extra-Str synaptic input.

**Key words:** acetylcholine; dopamine; fluorescence imaging; phosphorylated ribosomal protein S6; psychostimulant

## Significance Statement

Using the activity dependent marker phosphorylated ribosomal protein S6 (p-rpS6<sup>240/244</sup>), we mapped amphetamine (AMPH) effects on the activity of cholinergic interneurons (ChIs) across the striatum (Str). AMPH reduced ChI activity in dose-dependent manner in the ventral Str/nucleus accumbens (NAc), a critical site of psychostimulant action.

## Introduction

Psychostimulants such as amphetamine (AMPH) target dopamine (DA) neuron terminals (Sulzer, 2011) and engender dose-dependent behavioral effects. DA release in the ventral striatum/nucleus accumbens (Str/NAc) is associated with hyperlocomotion, whereas DA release in the dorsal Str is associated with stereotypies (Robinson and Becker, 1986; Kalivas and Stewart, 1991; Gaytan et al.,

1998; Yates et al., 2007). DA neurons modulate the activity of cholinergic interneurons (ChIs), which comprise <2% of striatal (Str) neurons, and yet strongly control the Str circuitry (Goldberg and Wilson, 2010; Gonzales and Smith, 2015; Abudukeyoumu et al., 2019). Modulation of ChI activity is critical for the processing and reinforcement of reward-related behaviors (Atallah et al., 2014; Gonzales and Smith, 2015). ChIs in the

Received May 3, 2021; accepted August 23, 2021; First published August 30, 2021.

The authors declare no competing financial interests.

Author contributions: S.Z. and S.R. designed research; S.Z., S.J.O., S.T., and S.F. performed research; S.Z., M.M., and J.B.-G. analyzed data; S.Z., N.C., and S.R. wrote the paper.

ventral Str are crucial for psychostimulant-dependent behaviors (Sofuoglu and Mooney, 2009; Witten et al., 2010; Lee et al., 2020; Lewis and Borrelli, 2020). However, whether AMPH has subregional effects on Chl activity has not been elucidated.

Previous studies have shown that the phosphorylated form of the ribosomal protein S6 at serine 240 and 244 residues (p-rpS6<sup>240/244</sup>) reports activity of Chls under different pharmacological and/or behavioral conditions (Bertran-Gonzalez et al., 2012; Kharkwal et al., 2016; Matamales et al., 2016a,b). The phosphorylation of rpS6 can be induced by multiple signaling cascades; mTORC1 pathway and/or mTORC1-independent pathways such as the PKC, the MAPK or the cAMP/PKA pathways (Valjent et al., 2011; Bertran-Gonzalez et al., 2012; Gangarossa and Valjent, 2012). The phosphorylation of rpS6 appears to occur sequentially at five serine residues: in the order 236, 235, 240, 244, and 247 (Knight et al., 2012; Biever et al., 2015a). Bertran-Gonzalez and colleagues showed a clear p-rpS6<sup>240/244</sup> signal preferentially expressed in Chls, in contrast to a much weaker signal of p-rpS6<sup>235/236</sup> (Bertran-Gonzalez et al., 2012). Pharmacological modification of Chl firing leads to changes of p-rpS6<sup>240/244</sup> intensity in Chls (Bertran-Gonzalez et al., 2012; Matamales et al., 2016b). To address regionality in AMPH modulation of Chl activity, we mapped p-rpS6<sup>240/244</sup> intensity in Chls throughout the entire rostrocaudal axis of the Str after a single low-dose or high-dose of AMPH at two time points: 2.5 h postinjection (2.5h<sub>pi</sub>) and 24 h postinjection (24h<sub>pi</sub>). This revealed that AMPH induces a delayed regionally heterogeneous dose-dependent attenuation of Chl activity in the ventral Str/NAc.

## Materials and Methods

### Ethics

This research was performed in accordance with the *Guide for the Care and Use of Laboratory Animals* of the National Institutes of Health, under a protocol approved by the Institutional Animal Care and Use Committee of New York State Psychiatric Institute (#NYSPI-1494).

### Experimental animals

Mice were 129Sv/C57BL6J mixed background, backcrossed to C57BL6J at least five times and kept inbred. Mice were group housed and maintained on a 12/12 h

This work was supported by National Institutes of Health Grants R01 DA038966 and R01 MH117128 (to S.R.), Philippe Foundation (to S.Z.), Australian Research Council Grants DP190102511 and DP210102700, and National Health and Medical Research Council Grants APP1165990 (to J.B.-G. and M.M.) and FT200100502 (to J.B.-G.).

Acknowledgements: We thank Susana Mingote, Leora Yetnikoff, and Vlad Velicu for technical help and advice.

Correspondence should be addressed to Samira Ztaou at [samira.ztaou@nyspi.columbia.edu](mailto:samira.ztaou@nyspi.columbia.edu) or Stephen Rayport at [stephen.rayport@nyspi.columbia.edu](mailto:stephen.rayport@nyspi.columbia.edu).

<https://doi.org/10.1523/ENEURO.0196-21.2021>

Copyright © 2021 Ztaou et al.

This is an open-access article distributed under the terms of the [Creative Commons Attribution 4.0 International license](https://creativecommons.org/licenses/by/4.0/), which permits unrestricted use, distribution and reproduction in any medium provided that the original work is properly attributed.

light/dark cycle with lights on at 7 A.M. in a temperature-controlled room with food and water provided *ad libitum*. The DAT-IRES-Cre/+;ROSA26-flox-STOP-CAG-ChR2-YFP double mutant strain (The Jackson Laboratory, RRID: [IMSR\\_JAX:006660](https://identifiers.org/IMSR_JAX:006660), RRID: [IMSR\\_JAX:024109](https://identifiers.org/IMSR_JAX:024109)) were used, with the same genotype as previous studies (Chuhma et al., 2014, 2018; Mingote et al., 2015, 2017). The presence of Cre is not essential for the present study; the IRES-cre transgene insertion in the DA transporter (DAT) locus modestly reduces DAT expression and AMPH responsiveness (Bäckman et al., 2006; Chohan et al., 2020).

For the immunocytochemistry experiments, 30 mice were used at postnatal day (P)56–P82, divided in two cohorts of 15 for 2.5h<sub>pi</sub> and 15 for 24h<sub>pi</sub>. Cohorts were balanced for sex: 16 male (2.5h<sub>pi</sub> cohort: saline, *n* = 3; low-dose AMPH, *n* = 3; high-dose AMPH, *n* = 3 and 24h<sub>pi</sub> cohort: saline, *n* = 2; low-dose AMPH, *n* = 2; high-dose AMPH, *n* = 3) and 14 female (2.5h<sub>pi</sub> cohort: saline, *n* = 2; low-dose AMPH, *n* = 2; high-dose AMPH, *n* = 2 and 24h<sub>pi</sub> cohort: saline, *n* = 3; low-dose AMPH, *n* = 3; high-dose AMPH, *n* = 2) mice. For the electrophysiological experiments, 40 male (saline, *n* = 17; low-dose AMPH, *n* = 11; high-dose AMPH, *n* = 12) and 40 female (saline, *n* = 13; low-dose AMPH, *n* = 11; high-dose AMPH, *n* = 16) mice at P52–P72 were used. No sex differences were observed, so data from male and female mice in each group were combined.

### Drug treatment

D-AMPH hemisulfate (Sigma-Aldrich, A5880) either low-dose (2 mg/kg) or high-dose (16 mg/kg) was dissolved in 0.9% NaCl immediately before use. Injections were done intraperitoneally at a volume of 10 ml/kg body weight.

### Behavioral monitoring

Mice were habituated to handling for 2 d before the drug administration. Monitoring took place under bright ambient light conditions during the light phase. On the injection day, mice were placed in the open field, equipped with infrared motion detectors (Plexiglas activity chambers, 40.6 cm long × 40.6 cm wide × 38.1 cm high; SmartFrame Open Field System, Kinder Scientific) for 1 h for habituation. Baseline activity was monitored for 30 min preinjection, then mice were injected intraperitoneally either with saline, 2 or 16 mg/kg AMPH, and observed for a 2-h postinjection period. Locomotor activity was recorded automatically in 10-min bins. Stereotyped behaviors, orofacial stereotypy (mouth movements, lick, bite, self-gnaw, taffy pull, jaw tremor, yawn) and grooming, were scored for 1 min every 5 min as previously described (Kelley, 2001).

### Immunocytochemistry

For immunocytochemistry, mice were deeply anesthetized with ketamine (90 mg/kg)/xylazine (7 mg/kg) and then perfused intracardially with cold PBS (100 mM; pH 7.4) followed by 4% paraformaldehyde (PFA). Brains were removed and postfixed overnight in 4% PFA. Coronal

sections were cut at 50  $\mu\text{m}$  with a vibrating microtome (Leica VT1200S), and stored in a cryoprotectant solution (30% glycerol, 30% ethylene glycol in 0.1 M Tris HCl, pH 7.4) at  $-20^{\circ}\text{C}$ . Free-floating sections were washed in PBS and incubated in glycine (100 mM) for 30 min to quench aldehydes. Non-specific binding was blocked with 10% normal donkey serum (NDS) in 0.1 PBS Triton X-100 for 2 h. Sections were incubated in PBS containing 0.02% Triton X-100 and 2% NDS overnight at  $4^{\circ}\text{C}$  with primary antibodies: anti-ChAT (1:500, goat polyclonal, Millipore catalog #AB144P, RRID:AB\_2079751) and anti-phosphorylated ribosomal protein S6 (p-rpS6<sup>240/244</sup>, 1:1500, rabbit polyclonal, Cell Signaling Technology catalog #2215, RRID:AB\_331682). Sections were then washed with PBS, and secondary antibodies applied for 45 min in PBS containing 0.02% Triton X-100 at room temperature: anti-goat Alexa Fluor 594 (1:200, Thermo Fisher Scientific catalog #A-11 058, RRID:AB\_2534105) and anti-rabbit Alexa Fluor 488 (1:200, Thermo Fisher Scientific catalog #A-21206, RRID:AB\_2535792). Sections were mounted on gelatin subbed slides (SouthernBiotech) and coverslipped with ProLong Gold aqueous medium with DAPI (Thermo Fisher Scientific) and stored at  $4^{\circ}\text{C}$  until imaging.

### Imaging and analysis

Images were acquired using an Axio Imager M2 fluorescence microscope (Zeiss) with a high-resolution digital camera (AxioCam 506 mono,  $2752 \times 2208$  pixels, Zeiss), a  $20\times/0.8$  objective and Zen 2.3 Digital Imaging software (Zeiss; RRID:SCR\_013672). Ten coronal sections, spanning the rostrocaudal extent of the right Str (bregma 1.54, 1.18, 0.98, 0.62, 0.26,  $-0.10$ ,  $-0.46$ ,  $-0.82$ ,  $-1.22$ , and  $-1.58$  mm), were imaged. An image stack consisting of 5 planes at 5  $\mu\text{m}$  intervals was obtained. Exposure time for each excitation was held constant throughout acquisition.

Raw 16-bit images were analyzed using Fiji/ImageJ (version 2.0.0., NIH, RRID:SCR\_002285). Z-projected images were obtained by taking pixels with the maximum intensity in a stack. The outer boundary of the Str and its anatomic subregions, NAc core and shell, dorsomedial (DM) Str and dorsolateral (DL) Str, were manually delineated in accordance with the mouse brain atlas (Paxinos and Franklin, 2008), and their areas ( $\text{mm}^2$ ) in each coronal section were obtained.

Particle analysis detected all ChAT-positive neurons in the Str and the total number of ChIs, perimeter ( $\mu\text{m}$ ), area ( $\mu\text{m}^2$ ), and circularity (a circularity value of 1 indicates a perfect circle while values approaching 0 indicate more elongated shapes) of each ChI were measured. Density of ChIs (neurons/ $\text{mm}^2$ ) in each Str subregion was calculated as ChI number in a subregion divided by area of the subregion. For each coronal section, the ChAT image was superimposed on the p-rpS6<sup>240/244</sup> image, and the ChAT-positive neurons were used as a mask for p-rpS6<sup>240/244</sup> intensity analysis. Fluorescence intensity of the corpus callosum was used for background subtraction.

Location of each ChI was defined by coordinates of the centroid. The p-rpS6<sup>240/244</sup> intensity of each ChI was normalized to the maximum and the minimum intensities for each cohort,  $2.5h_{\text{pi}}$  or  $24h_{\text{pi}}$ , and color-scaled. All color-

scaled ChIs were 3D plotted with outlines of the Str using a customized script in MATLAB (MathWorks; RRID:SCR\_001622) as previously described (Matamales et al., 2016a).

Distributions of p-rpS6<sup>240/244</sup> fluorescence intensity were standardized to the corresponding saline group for each time point and subregion by calculating z-scores:  $z = (x - \mu)/\sigma$ , where  $x$  is the p-rpS6<sup>240/244</sup> signal in individual ChIs,  $\mu$  and  $\sigma$  are the mean and the SD, respectively, of p-rpS6<sup>240/244</sup> signal in the corresponding saline group.

### Slice electrophysiology and analysis

For electrophysiology recording, mice were anesthetized with ketamine (90 mg/kg)/xylazine (7 mg/kg). After confirmation of full anesthesia, mice were decapitated and brains quickly removed in ice-cold high-glucose artificial CSF (ACSF; 75 mM NaCl, 2.5 mM KCl, 25 mM NaHCO<sub>3</sub>, 1.25 mM NaH<sub>2</sub>PO<sub>4</sub>, 0.7 mM CaCl<sub>2</sub>, 2 mM MgCl<sub>2</sub>, and 100 mM glucose; pH 7.4) saturated with carbogen (95% O<sub>2</sub> + 5% CO<sub>2</sub>). Coronal sections of the Str (bregma from 1.70 to 0.26 mm) were cut, 300  $\mu\text{m}$  thick, with a vibrating microtome (VT1200S, Leica), incubated in high-glucose ACSF at room temperature for at least 1 h for recovery, then transferred to the recording chamber (submerged, 500  $\mu\text{l}$  volume) on the stage of an upright microscope (BX61WI, Olympus), continuously perfused with standard ACSF (125 mM NaCl, 2.5 mM KCl, 25 mM NaHCO<sub>3</sub>, 1.25 mM NaH<sub>2</sub>PO<sub>4</sub>, 2 mM CaCl<sub>2</sub>, 1 mM MgCl<sub>2</sub>, and 25 mM glucose; pH 7.4) saturated with carbogen. Recorded neurons were visualized using enhanced visible light differential interference contrast (DIC) optics with a scientific c-MOS camera (ORCA-Flash4.0LT, Hamamatsu Photonics).

ChIs were identified visually by large soma size, confirmed by spontaneous firing, shallow resting membrane potentials (around 60 mV) and voltage sag by  $-400$  pA current injection (700 ms in duration; Chuhma et al., 2014, 2018). Recording patch pipettes were fabricated from standard-wall borosilicate glass capillary with filament (World Precision Instruments). Pipette resistance was 4–9 M $\Omega$  and series resistance was 7–32 M $\Omega$ . Composition of intracellular solution was 135 mM K<sup>+</sup>-methane sulfonate (MeSO<sub>4</sub>), 5 mM KCl, 2 mM MgCl<sub>2</sub>, 0.1 mM CaCl<sub>2</sub>, 10 mM HEPES, 1 mM EGTA, 2 mM ATP, and 0.1 mM GTP; pH 7.25. Recording was done with an Axopatch 200B amplifier (Molecular Devices) in fast current clamp mode. All recordings were done at  $32$ – $34^{\circ}\text{C}$  (TC 344B Temperature Controller, Warner Instruments). No more than four cells were recorded per animal.

Data were filtered at 5 kHz using a four-pole Bessel filter, digitized at 5 kHz (Digidata 1550A, Molecular Devices) and recorded using pClamp 10 (Molecular Devices; RRID:SCR\_011323). Electrophysiological data were analyzed with Axograph X (Axograph Science; RRID:SCR\_014284). Firing frequencies were calculated as average frequency in a 2 s window obtained from 10 consecutive traces.

### Statistical analysis

Sample sizes were determined using G\*Power 3.1 with effect sizes based on similar experiments (G\*Power,

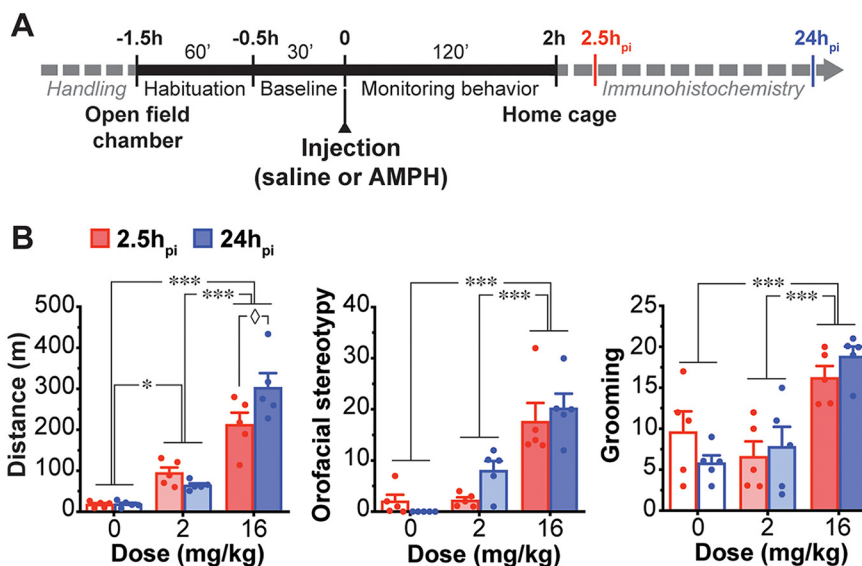


**Figure 1.** Dose-dependent behavioral effects of AMPH. **A**, Timeline of AMPH experiments. **B**, Total distance traveled (left), orofacial stereotypy (middle), and grooming (right) scores are shown after saline (0 mg/kg,  $n = 5$  animals), low-dose (2 mg/kg,  $n = 5$  animals), or high-dose (16 mg/kg,  $n = 5$  animals) AMPH, for 2.5h<sub>pi</sub> cohort (red) and 24h<sub>pi</sub> cohort (blue). Dots in bar graphs show measurements per animal. \* $p < 0.05$ , \*\* $p < 0.01$ , \*\*\* $p < 0.001$  for comparison among doses;  $\diamond p < 0.05$  for comparison between 2.5h<sub>pi</sub> and 24h<sub>pi</sub>.

RRID: SCR\_013726), setting  $\alpha = 0.05$  and power = 0.8 (Cunningham and McCrum-Gardner, 2007; Faul et al., 2007). For the immunocytochemistry experiments, we used Cohen's  $d = 0.97$  as an effect size, resulting in 5 mice per group. For the electrophysiological experiments, we used Cohen's  $d = 0.32$  as an effect size, resulting in 12 mice per group.

Statistical analyses were performed using Prism 8 (GraphPad Prism, RRID:SCR\_002798) or SPSS 26 (SPSS; RRID:SCR\_002865).  $p < 0.05$  was considered as significant for all analyses. Data are presented as mean  $\pm$  SEM. Parametric tests were used here because datasets followed a normal distribution (D'Agostino–Pearson normality test,  $p > 0.05$ ). ANOVA was used for comparison among conditions. Where significance was detected, multiple pairwise comparisons with Bonferroni correction were performed as *post hoc* tests.

## Results

### Dose-dependent effects of AMPH on locomotor activity and stereotypy

Behavioral observations were used to confirm the dose-dependent effects of AMPH. Mice received a single low-dose (2 mg/kg) or high-dose (16 mg/kg) of AMPH, and their brains were extracted for analysis either after 2.5h<sub>pi</sub>, when acute behavioral effects had subsided, or at 24h<sub>pi</sub> to assess enduring effects on Ch1 activity in the Str. One low-dose AMPH-injected mouse, in the 2.5h<sub>pi</sub> cohort, was excluded from the study as its locomotor activity decreased after injection.

To confirm differential behavioral effects of the two AMPH doses and similar behavioral effects in the two cohorts (2.5h<sub>pi</sub> and 24h<sub>pi</sub>), mice from each cohort received saline, low-dose or high-dose AMPH, and locomotion and

stereotypy were monitored for 2 h in the open field (Fig. 1A). Total travel distance dose dependently increased in both the 2.5h<sub>pi</sub> cohort (saline  $17.6 \pm 3.4$  m, low-dose  $94.5 \pm 13.8$  m, high-dose  $212.5 \pm 29.3$  m) and 24h<sub>pi</sub> cohort (saline  $18.6 \pm 3.4$  m, low-dose  $64.0 \pm 5.0$  m, high-dose  $302.7 \pm 35.8$  m), while no significant difference was observed between the two cohorts (two-way ANOVA; treatment effect,  $F_{(2,24)} = 78.15$ ,  $p < 0.001$ ; cohort effect,  $F_{(1,24)} = 1.55$ ,  $p = 0.23$ ; Fig. 1B, left). Although there was a significant treatment  $\times$  cohort interaction ( $F_{(2,24)} = 4.95$ ,  $p = 0.02$ ), the two cohorts showed similar dose-dependent hyperlocomotion, a significant increase after low-dose and a further increase after high-dose.

Low-dose and high-dose AMPH increased orofacial stereotypy in both the 2.5h<sub>pi</sub> cohort (saline  $2.0 \pm 1.3$ , low-dose  $2.2 \pm 0.6$ , high-dose  $17.6 \pm 3.6$ ) and 24h<sub>pi</sub> cohort (saline  $0 \pm 0$ , low-dose  $8.0 \pm 1.9$ , high-dose  $20.2 \pm 2.9$ ), while no significant difference was observed between the two cohorts (two-way ANOVA; treatment effect,  $F_{(2,24)} = 38.74$ ,  $p < 0.001$ ; cohort effect,  $F_{(1,24)} = 1.50$ ,  $p = 0.23$ ; treatment  $\times$  cohort interaction,  $F_{(2,24)} = 1.69$ ,  $p = 0.21$ ; Fig. 1B, middle).

Low-dose AMPH did not affect grooming score in the two cohorts, while high-dose increased it in both 2.5h<sub>pi</sub> cohort (saline  $9.6 \pm 2.5$ , low-dose  $6.6 \pm 1.9$ , high-dose  $16.2 \pm 1.5$ ) and 24h<sub>pi</sub> cohort (saline  $5.8 \pm 0.9$ , low-dose  $7.8 \pm 2.4$ , high-dose  $18.8 \pm 1.2$ ; two-way ANOVA; treatment effect,  $F_{(2,24)} = 19.86$ ,  $p < 0.001$ ). Neither a significant difference, nor a treatment  $\times$  cohort interaction, was observed between the two cohorts (cohort effect,  $F_{(1,24)} = 0$ ,  $p > 0.99$ ; treatment  $\times$  cohort interaction,  $F_{(2,24)} = 1.67$ ,  $p = 0.21$ ; Fig. 1B, right). These observations confirmed that AMPH elicited a comparable dose-dependent behavioral activation in the two cohorts, used for the 2.5h<sub>pi</sub> and 24h<sub>pi</sub> Ch1 studies.

## Distribution and morphology of ChIs is not affected by AMPH

To address potential neurotoxic effects of AMPH on ChIs, particularly high-dose (viz., Zhu et al., 2006), we examined ChI distribution and soma morphology. ChIs were identified by ChAT immunostaining and examined in 10 coronal sections spanning the rostrocaudal extent of the right Str in four subregions: NAc core and shell, DM and DL Str (Fig. 2A). The previously recognized rostro-caudal distribution of ChIs (Matamalas et al., 2016a) peaked at 0.98 mm from bregma and gradually declined caudally. The distribution was not affected by either AMPH dose or time after injection (three-way ANOVA; rostrocaudal effect,  $F_{(9,240)} = 204.13$ ,  $p < 0.001$ ; treatment effect,  $F_{(2,240)} = 0.17$ ,  $p = 0.85$ ; time effect,  $F_{(1,240)} = 0.66$ ,  $p = 0.42$ ; rostrocaudal  $\times$  treatment  $\times$  time interaction,  $F_{(18,240)} = 1.43$ ,  $p = 0.12$ ; Fig. 2B). Although numbers of ChIs varied significantly between Str subregions, AMPH dose or time after injection did not affect ChI count significantly in any Str subregion (three-way ANOVA; location effect,  $F_{(3,96)} = 954.82$ ,  $p < 0.001$ ; treatment effect,  $F_{(2,96)} = 0.12$ ,  $p = 0.89$ ; time effect,  $F_{(1,96)} = 0.42$ ,  $p = 0.52$ ; location  $\times$  treatment  $\times$  time interaction,  $F_{(6,96)} = 0.52$ ,  $p = 0.80$ ; Fig. 2C, top). Although ChI densities varied between Str subregions, highest in the NAc shell and lowest in the NAc core, AMPH dose or time after injection did not affect densities in any subregion (three-way ANOVA; location effect,  $F_{(3,96)} = 73.76$ ,  $p < 0.001$ ; treatment effect,  $F_{(2,96)} = 0.15$ ,  $p = 0.86$ ; time effect,  $F_{(1,96)} = 0.57$ ,  $p = 0.45$ ; location  $\times$  treatment  $\times$  time interaction,  $F_{(6,96)} = 0.30$ ,  $p = 0.94$ ; Fig. 2C, bottom).

We examined the shape of ChIs based on their cytoplasmic ChAT immunoreactivity. AMPH did not affect ChI soma area (2.5h<sub>pi</sub>: saline  $242.5 \pm 4.4 \mu\text{m}^2$ , low-dose  $243.6 \pm 10.5 \mu\text{m}^2$ , high-dose  $240.4 \pm 9.6 \mu\text{m}^2$ ; 24h<sub>pi</sub>: saline  $242.6 \pm 14.6 \mu\text{m}^2$ , low-dose  $250.1 \pm 3.0 \mu\text{m}^2$ , high-dose  $242.5 \pm 5.5 \mu\text{m}^2$ ; two-way ANOVA; treatment effect,  $F_{(2,24)} = 0.21$ ,  $p = 0.81$ ; time effect,  $F_{(1,24)} = 0.16$ ,  $p = 0.69$ ; treatment  $\times$  time interaction,  $F_{(2,24)} = 0.07$ ,  $p = 0.94$ ), perimeter (2.5h<sub>pi</sub>: saline  $72.3 \pm 1.4 \mu\text{m}$ , low-dose  $74.3 \pm 3.4 \mu\text{m}$ , high-dose  $75.3 \pm 3.1 \mu\text{m}$ ; 24h<sub>pi</sub>: saline  $76.3 \pm 1.1 \mu\text{m}$ , low-dose  $75.6 \pm 1.4 \mu\text{m}$ , high-dose  $76.3 \pm 1.4 \mu\text{m}$ ; two-way ANOVA; treatment effect,  $F_{(2,24)} = 0.23$ ,  $p = 0.80$ ; time effect,  $F_{(1,24)} = 1.44$ ,  $p = 0.24$ ; treatment  $\times$  time interaction,  $F_{(2,24)} = 0.29$ ,  $p = 0.75$ ) or circularity (2.5h<sub>pi</sub>: saline  $0.60 \pm 0.02$ , low-dose  $0.59 \pm 0.04$ , high-dose  $0.56 \pm 0.03$ ; 24h<sub>pi</sub>: saline  $0.56 \pm 0.04$ , low-dose  $0.58 \pm 0.04$ , high-dose  $0.55 \pm 0.04$ ; two-way ANOVA; treatment effect,  $F_{(2,24)} = 0.28$ ,  $p = 0.76$ ; time effect,  $F_{(1,24)} = 0.56$ ,  $p = 0.46$ ; treatment  $\times$  time interaction,  $F_{(2,24)} = 0.07$ ,  $p = 0.93$ ) in the whole Str, at any time points (Fig. 3A).

Although ChI morphology differed between Str subregions, AMPH did not affect soma area, perimeter, or circularity in any Str subregion or at the two different time points (area: three-way ANOVA; location effect,  $F_{(3,96)} = 13.17$ ,  $p < 0.001$ ; treatment effect,  $F_{(2,96)} = 0.37$ ,  $p = 0.68$ ; time effect,  $F_{(1,96)} = 0.31$ ,  $p = 0.58$ ; location  $\times$  treatment  $\times$  time interaction,  $F_{(6,96)} = 0.18$ ,  $p = 0.98$ ; perimeter: three-way ANOVA; location effect,  $F_{(3,96)} = 22.45$ ,  $p < 0.001$ ; treatment effect,  $F_{(2,96)} = 0.38$ ,  $p = 0.68$ ; time effect,

$F_{(1,96)} = 2.42$ ,  $p = 0.12$ ; location  $\times$  treatment  $\times$  time,  $F_{(6,96)} = 0.83$ ,  $p = 0.55$ ; circularity: three-way ANOVA; location effect,  $F_{(3,96)} = 7.69$ ,  $p < 0.001$ ; treatment effect,  $F_{(2,96)} = 0.58$ ,  $p = 0.57$ ; time effect,  $F_{(1,96)} = 1.36$ ,  $p = 0.25$ ; location  $\times$  treatment  $\times$  time interaction,  $F_{(6,96)} = 0.35$ ,  $p = 0.91$ ; Fig. 3B). Thus, neither low- nor high-dose AMPH affected ChI distribution or morphology, arguing against neurotoxic effects of a single dose of AMPH.

## AMPH attenuation of ChI activity *in vivo*

We mapped AMPH effects on ChI activity using p-rpS6<sup>240/244</sup> as a reporter. Double immunostaining showed colocalization of ChAT and p-rpS6<sup>240/244</sup> (Fig. 4). P-rpS6<sup>240/244</sup> signal was also present in other Str cells, so ChAT staining was used to extract the signal specifically deriving from ChIs. We quantified p-rpS6<sup>240/244</sup> intensity as the average pixel intensity in each ChAT-positive neuron, in sections from the saline, low-dose and high-dose AMPH-injected mice, at 2.5h<sub>pi</sub> or 24h<sub>pi</sub> ( $n = 5$  animals/treatment, 10 hemisections/animal). Individual ChI locations were plotted in coronal hemisections of the Str and p-rpS6<sup>240/244</sup> intensities were color-scaled (Fig. 5A,C).

At 2.5h<sub>pi</sub>, p-rpS6<sup>240/244</sup> intensity varied among Str subregions, with higher p-rpS6<sup>240/244</sup> intensity in the DM Str decreasing ventrally to the NAc shell (Fig. 5A). There was no apparent difference in the distribution of p-rpS6<sup>240/244</sup> intensity between saline, low-dose, and high-dose AMPH-injected animals (Fig. 5A). Average p-rpS6<sup>240/244</sup> intensity in the whole Str did not differ among saline, low-dose and high-dose AMPH-injected animals (one-way ANOVA,  $F_{(2,12)} = 0.003$ ,  $p = 0.99$ ; Fig. 5B, left). Although average ChI p-rpS6<sup>240/244</sup> intensities differed in Str subregions, neither low- nor high-dose AMPH affected ChI p-rpS6<sup>240/244</sup> intensity in any Str subregion at 2.5h<sub>pi</sub> (two-way ANOVA; treatment effect,  $F_{(2,48)} = 0.62$ ,  $p = 0.54$ ; location effect,  $F_{(3,48)} = 41.28$ ,  $p < 0.001$ ; treatment  $\times$  location interaction,  $F_{(6,48)} = 0.66$ ,  $p = 0.68$ ; Fig. 5B, right).

At 24h<sub>pi</sub>, ChI p-rpS6<sup>240/244</sup> intensity was reduced by low-dose AMPH particularly in the NAc (Fig. 5C). Low-dose AMPH reduced p-rpS6<sup>240/244</sup> staining more than high-dose (Fig. 5C). Indeed, low-dose AMPH reduced average ChI p-rpS6<sup>240/244</sup> staining in the whole Str, while high-dose AMPH did not show a significant effect (one-way ANOVA,  $F_{(2,12)} = 4.35$ ,  $p = 0.03$ ; Fig. 5D, left). Low-dose AMPH significantly reduced ChI p-rpS6<sup>240/244</sup> intensity in the NAc core ( $p = 0.043$ ) and NAc shell ( $p = 0.047$ ), but not in the dorsal Str (DM Str,  $p = 0.46$ ; DL Str,  $p = 0.40$ ; Fig. 5D, right; two-way ANOVA; treatment effect,  $F_{(2,48)} = 8.56$ ,  $p < 0.001$ ; location effect,  $F_{(3,48)} = 0.20$ ,  $p = 0.89$ ; treatment  $\times$  location interaction,  $F_{(6,48)} = 0.35$ ,  $p = 0.91$ ). High-dose AMPH does not affect ChI p-rpS6<sup>240/244</sup> intensity in any Str subregion.

To compare AMPH effects on p-rpS6<sup>240/244</sup> intensity between the two time points, p-rpS6<sup>240/244</sup> intensities in ChIs were standardized to the respective saline groups and the differences expressed as z-scores for each Str subregion. Z-scores in AMPH-injected animals at 2.5h<sub>pi</sub> showed no difference from saline-injected animals in any Str subregion (two-way ANOVA; treatment effect  $F_{(2,48)} = 0.70$ ,  $p = 0.50$ ; location effect  $F_{(3,48)} = 1.98$ ,  $p = 0.13$ ;

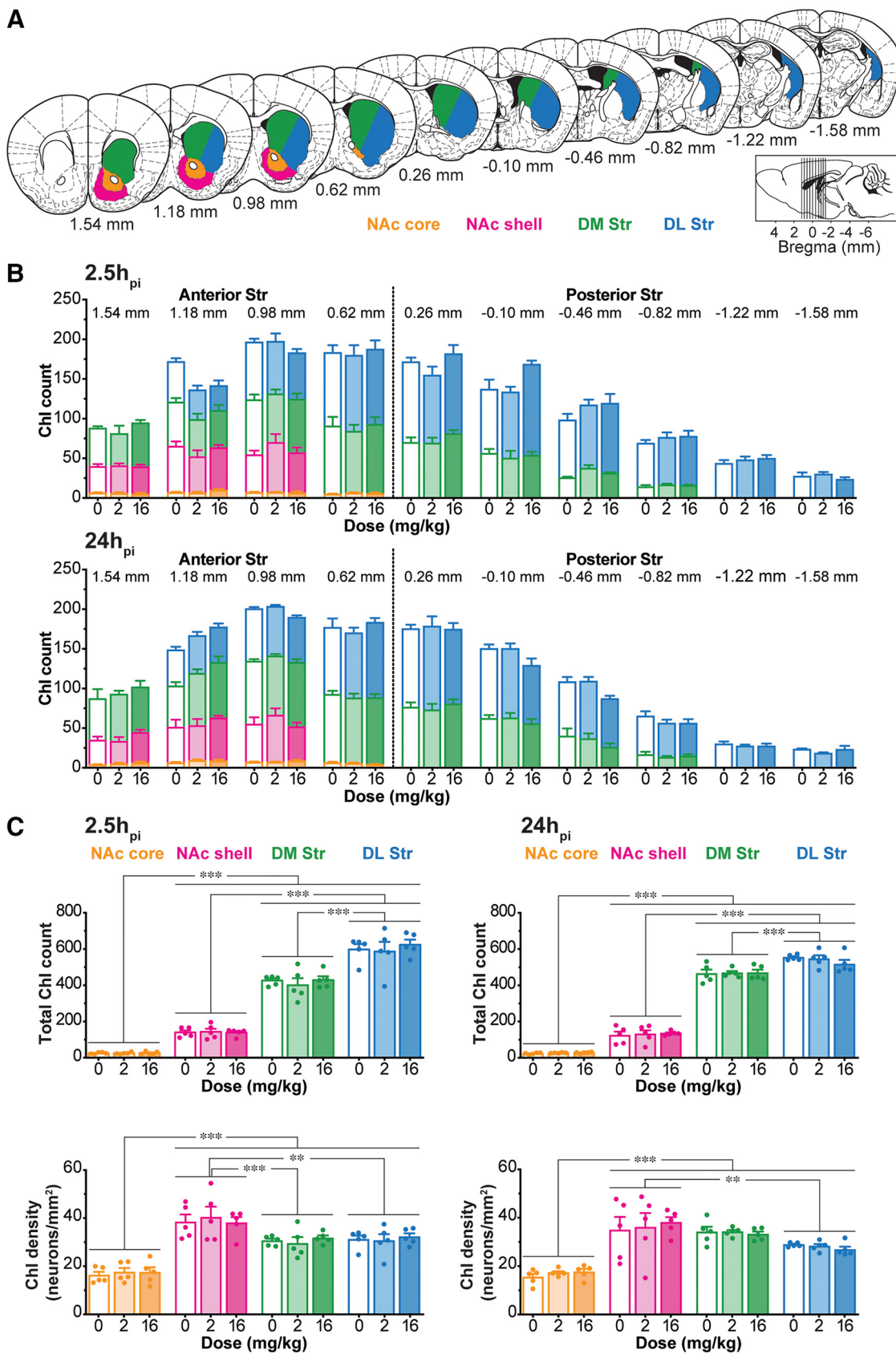


**Figure 2.** Distribution of Chls in the Str is not affected by AMPH. **A**, Schematic representations of 10 coronal sections of the Str (from bregma +1.54 to -1.58 mm). Delineations of Str subregions are shown in the right Str (Paxinos and Franklin, 2008): NAc core

continued

(orange), NAc shell (magenta), DM Str (green), DL Str (blue). Locations of slices are shown in inset, and locations from bregma are indicated under the slices. **B**, Stacked bar graphs showing counts of ChIs across Str subregions in 10 coronal hemisections along the rostrocaudal axis after saline (0 mg/kg), low-dose (2 mg/kg), or high-dose (16 mg/kg) AMPH, at 2.5h<sub>pi</sub> (top) and 24h<sub>pi</sub> (bottom). **C**, Total ChI count (top) and ChI density (neurons/mm<sup>2</sup>; bottom) in each Str subregion are shown, at 2.5h<sub>pi</sub> (left) and 24h<sub>pi</sub> (right). Group *ns* are given in Figure 1. Dots in bar graphs show the average per animal; \*\**p* < 0.01 and \*\*\**p* < 0.001.

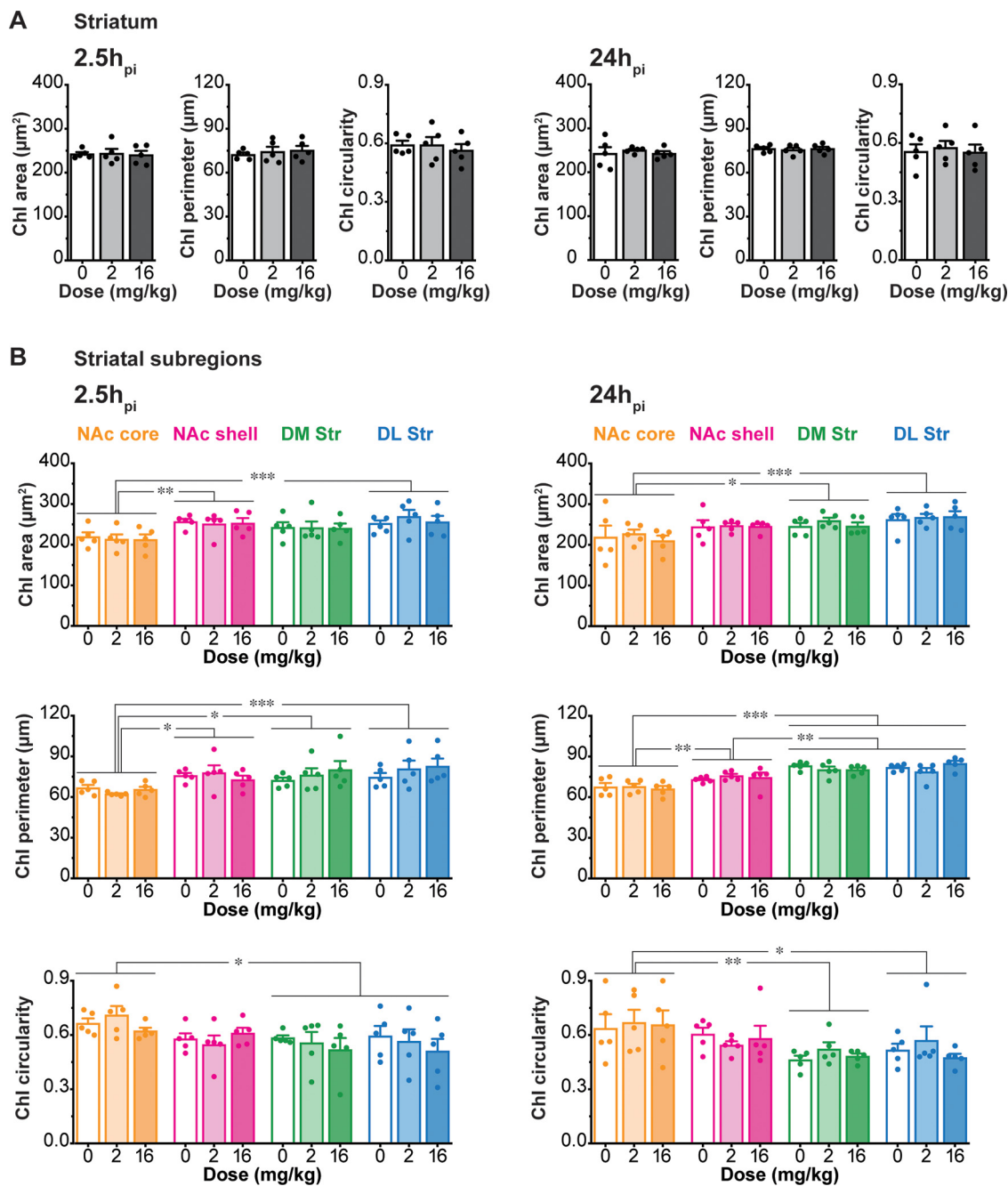


**Figure 3.** Morphology of ChIs is not affected by AMPH. **A–B**, Morphologic characteristics of ChIs in the whole Str (**A**) and each Str subregion (**B**) in the same hemisections as shown in the previous figure: area (µm<sup>2</sup>), perimeter (µm), and circularity after saline (0 mg/kg), low-dose (2 mg/kg), or high-dose (16 mg/kg) AMPH, at 2.5h<sub>pi</sub> (left) and 24h<sub>pi</sub> (right). Dots in bar graphs show the average measurements per animal; \**p* < 0.05, \*\**p* < 0.01, \*\*\**p* < 0.001.

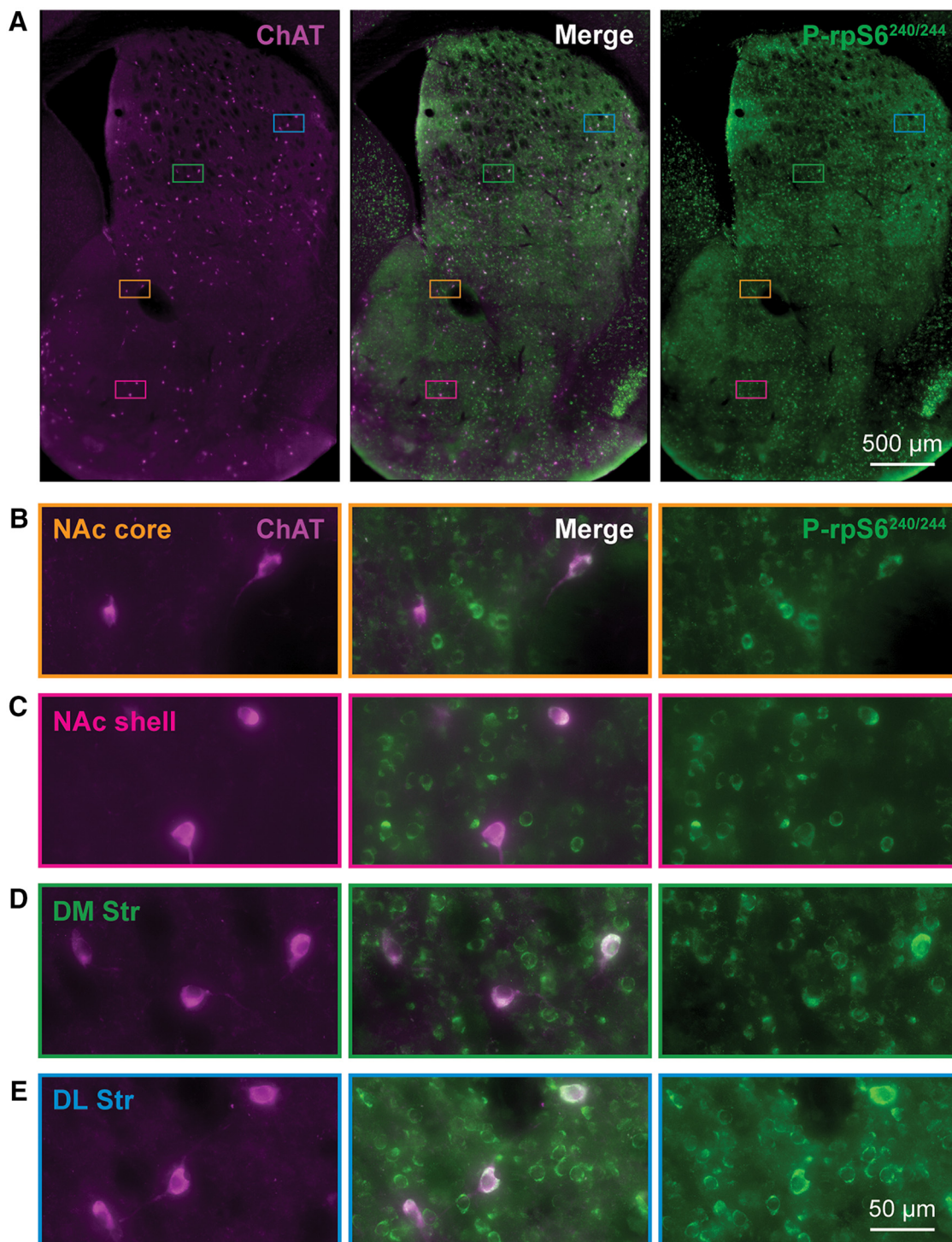


**Figure 4.** Phosphorylation of ribosomal protein S6 (p-rpS6<sup>240/244</sup>) in Chls. **A**, Low-magnification images of ChAT (purple) and p-rpS6<sup>240/244</sup> (green) in a Str hemisection (bregma 0.98 mm) with merged images in the middle. Colored rectangles are representative locations of Str subregions and magnified in **B–E**. Expanded images of the NAc core (**B**, orange), NAc shell (**C**, magenta), DM Str (**D**, green), and DL Str (**E**, blue) subregions.

treatment  $\times$  location interaction,  $F_{(6,48)} = 0.65$ ,  $p = 0.69$ ; Fig. 6A). At 24h<sub>pi</sub>, p-rpS6<sup>240/244</sup> intensity z-scores became negative after low-dose or high-dose AMPH in all Str subregions, indicating a reduction in Chl activity (two-way ANOVA; treatment effect  $F_{(2,48)} = 8.97$ ,  $p < 0.001$ ; location

effect  $F_{(3,48)} = 0.54$ ,  $p = 0.66$ ; treatment  $\times$  location interaction,  $F_{(6,48)} = 0.49$ ,  $p = 0.81$ ; Fig. 6B). Low-dose AMPH significantly attenuated Chl p-rpS6<sup>240/244</sup> intensity z-scores in the ventral subregions: NAc core ( $p = 0.012$ ) and shell ( $p = 0.048$ ), but not in the dorsal Str (DM Str,  $p = 0.50$ ; DL



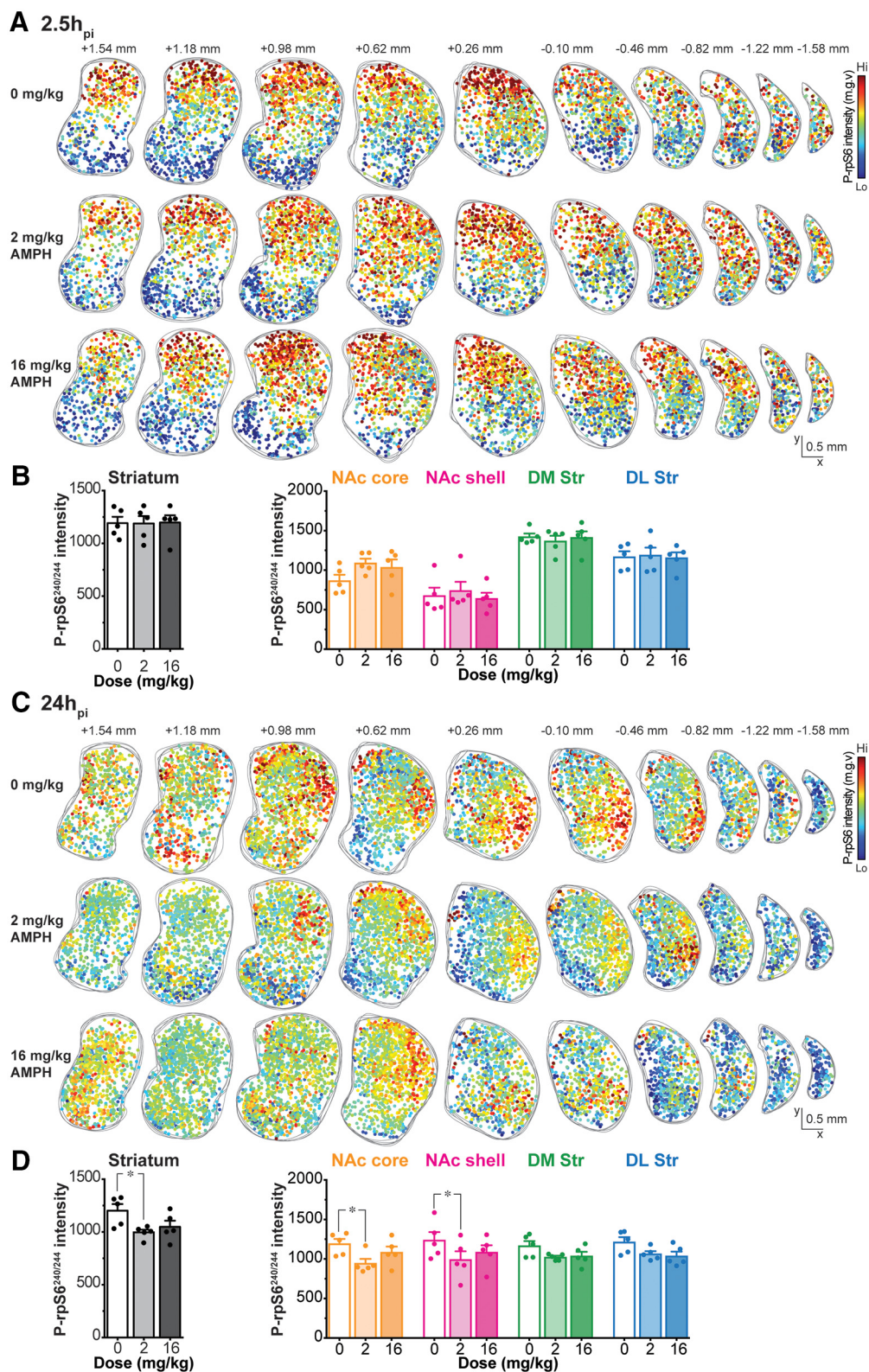


**Figure 5.** P-rpS6<sup>240/244</sup> intensity in Chls 2.5h<sub>pi</sub> and 24h<sub>pi</sub> AMPH. **A, C**, Spatial distribution of Chls with relative p-rpS6<sup>240/244</sup> intensity in the same 10 hemisections as shown in the previous morphology figures along the rostrocaudal axis (from bregma +1.54 to -1.58 mm), at 2.5h<sub>pi</sub> (**A**) and 24h<sub>pi</sub> (**C**). Spatial distribution of Chls from five animals was superimposed for each injection group: saline (top), low-dose (middle), or high-dose (bottom) AMPH. Each dot represents one Chl and intensity of p-rpS6<sup>240/244</sup> is shown on a blue (low level) to red (high level) color scale. **B, D**, left, Average p-rpS6<sup>240/244</sup> intensity in Chls in the whole Str at 2.5h<sub>pi</sub> (**B**) and 24h<sub>pi</sub> (**D**) after saline (0 mg/kg), low-dose (2 mg/kg), or high-dose (16 mg/kg) AMPH. Right, Box and whiskers plots showing p-rpS6<sup>240/244</sup> intensity in Chls in each Str subregion at 2.5h<sub>pi</sub> (**B**) and 24h<sub>pi</sub> (**D**). Dots in bar graphs show the average measurements per animal; \**p* < 0.05.

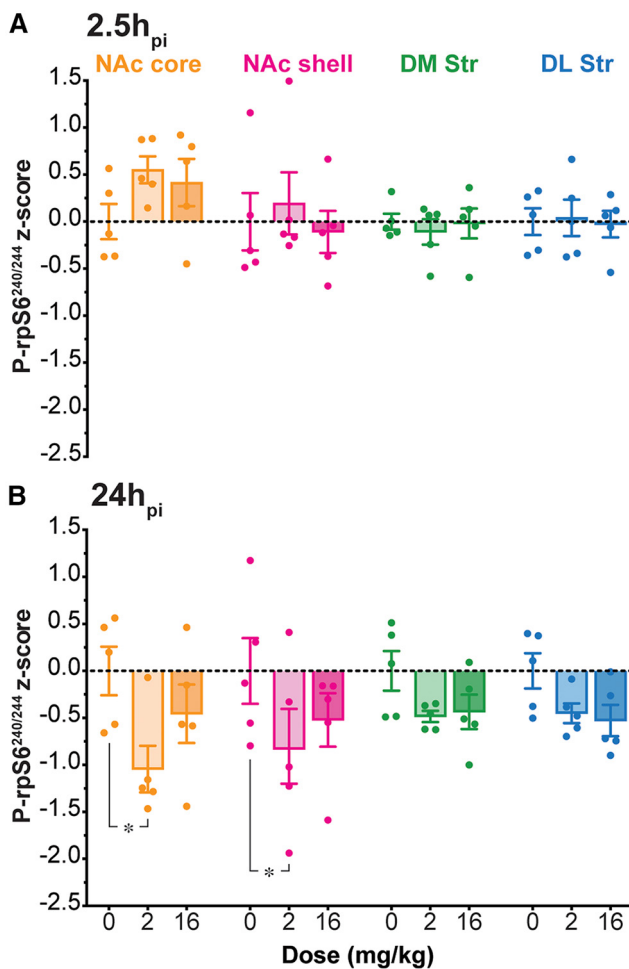


**Figure 6.** Comparison of p-rpS6<sup>240/244</sup> intensity in ChIs 2.5h<sub>pi</sub> and 24h<sub>pi</sub> AMPH. **A, B**, Comparison of ChI p-rpS6<sup>240/244</sup> intensity z-scores compared to the mean intensity in the corresponding saline-injected animals at 2.5h<sub>pi</sub> (**A**) and 24h<sub>pi</sub> (**B**) of saline (0 mg/kg), low-dose (2 mg/kg), or high-dose (16 mg/kg) AMPH in each Str subregion. Dots in bar graphs show the average measurements per animal; \* $p < 0.05$ .

Str,  $p = 0.60$ ; Fig. 6B). AMPH effects on z-scores at 24h<sub>pi</sub> were significantly different from those at 2.5h<sub>pi</sub> (three-way ANOVA; time effect,  $F_{(1,96)} = 27.35$ ,  $p < 0.001$ ; treatment effect,  $F_{(2,96)} = 3.18$ ,  $p = 0.04$ ; location effect,  $F_{(3,96)} = 0.34$ ,  $p = 0.80$ ; time  $\times$  treatment  $\times$  location interaction,  $F_{(6,96)} = 0.89$ ,  $p = 0.51$ ).

The two doses did not affect ChI p-rpS6<sup>240/244</sup> intensity in the dorsal subregions (Fig. 6B), nor was there any difference between the medial and lateral subregions. In the ventral subregions, the NAc core showed a similar profile of attenuation to the NAc shell. This medio-lateral concordance in the dorsal and ventral Str reinforces the differential effect in the ventral Str. The difference between the 2.5h<sub>pi</sub> and 24h<sub>pi</sub> cohorts reveals a time-dependent effect of a single dose of AMPH on ChI activity in the Str.

### Spontaneous firing of ChIs is not affected by AMPH

To investigate possible mechanisms underlying the observed decrease in p-rpS6<sup>240/244</sup>, we recorded

spontaneous firing of ChIs in slices in the four Str subregions after saline, low-dose or high-dose AMPH at 24h<sub>pi</sub> (Fig. 7A). ChIs were identified visually by large soma size, confirmed by spontaneous firing and voltage sag in response to hyperpolarizing-current injection (Fig. 7B), as described previously (Chuhma et al., 2014). Although firing frequencies of ChIs varied significantly among Str subregions, AMPH did not affect firing frequencies of ChIs in any Str subregion (two-way ANOVA; treatment effect,  $F_{(2,134)} = 1.21$ ,  $p = 0.30$ ; location effect,  $F_{(3,134)} = 13.30$ ,  $p < 0.001$ ; treatment  $\times$  location interaction,  $F_{(6,134)} = 1.12$ ,  $p = 0.36$ ; Fig. 7C). Thus, neither low- nor high-dose AMPH affected the intrinsic firing of ChIs in the deafferented slice, at 2.5h<sub>pi</sub> or 24h<sub>pi</sub>, suggesting AMPH effects on ChI activity are because of extra-Str synaptic input.

### Discussion

ChIs are principal targets of DA neurons and subject to regionally heterogeneous modulation. Here, we mapped the downstream effects of a single AMPH dose on ChI activity using p-rpS6<sup>240/244</sup> as a ChI-preferential activity-dependent marker. The single dose of AMPH did not affect the distribution, overall morphology, or spontaneous firing of ChIs in any Str subregion, arguing against neurotoxic effects of AMPH. While AMPH had no effect on *in vivo* ChI activity at 2.5h<sub>pi</sub>, it significantly attenuated ChI activity at 24h<sub>pi</sub> in the ventral Str/NAc. In the NAc, the attenuation in ChI activity after low-dose was greater than after high-dose. In the dorsal Str, no significant difference in ChI activity was observed after either low-dose or high-dose AMPH. Thus, a single dose of AMPH has delayed regionally heterogeneous effects on ChI activity, with a dose-dependency in the NAc.

### Distribution, morphology, and spontaneous firing of ChIs in the Str

In rodents (Gonzales and Smith, 2015), non-human primates (Brauer et al., 2000) and humans (Holt et al., 1996), the average size of ChIs in the NAc is smaller than in the dorsal Str. Here, we found that ChIs in the NAc core were significantly smaller and more elongated compared with those in other Str subregions, and that the morphology of ChIs soma (area, perimeter and circularity) differed among Str subregions. We also confirmed the differential distribution of ChIs in Str subregions (Gonzales and Smith, 2015). ChIs are denser in the NAc medial shell, as previously described in mice (Matamales et al., 2016a), rats (Phelps and Vaughn, 1986), and primates (Brauer et al., 2000).

A single injection of AMPH, either low-dose or high-dose, did not affect ChI distribution or soma morphology in any Str subregion, at either time point, showing these doses were not neurotoxic. Although AMPH neurotoxicity on DA neurons has been known for some time (Wagner et al., 1980; Ricaurte et al., 1984; Ryan et al., 1990; Miller and O'Callaghan, 1996; Krasnova et al., 2001, 2005; Granado et al., 2018), no study has focused on downstream neurotoxic effect on Str ChIs. To cause a significant toxic effect on ChIs, a higher dose of a more potent psychostimulant appears to be required; a single high-

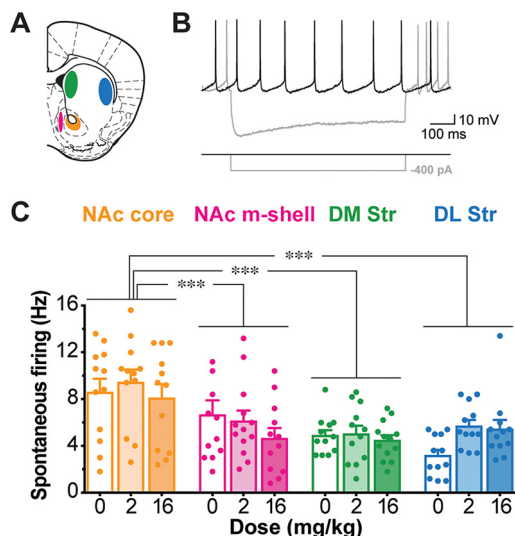


**Figure 7.** Spontaneous Chl firing 24h<sub>pi</sub> AMPH. **A**, Whole-cell recordings were made from Chls in the four Str subregions. **B**, An example of Chl firing recorded in the DL Str shows the characteristic spontaneous firing (black trace), and the prominent sag in response to hyperpolarizing-current injection (gray trace). **C**, Spontaneous firing frequencies of Chls in each Str subregion are shown after saline (0 mg/kg,  $n=30$  animals), low-dose (2 mg/kg,  $n=22$  animals), or high-dose (16 mg/kg,  $n=28$  animals) AMPH at 24h<sub>pi</sub>. Dots in bar graphs show measurements for individual animals; the numbers of Chls recorded were 12–13 cells/Str subregion/treatment; \*\*\* $p < 0.001$ .

dose (30 mg/kg) of methamphetamine was found to induce a loss of 29% of Chls in the dorsal Str (Zhu et al., 2006; Goodwin et al., 2009).

Although Chl spontaneous firing rates differed among Str subregions (Chuhma et al., 2014; Gonzales and Smith, 2015), a previous study found that a single dose of AMPH at 2.5h<sub>pi</sub> did not affect intrinsic firing of Chls in any Str subregion (Chuhma et al., 2014). Here, we have found that a single dose of AMPH at 24h<sub>pi</sub>, either low-dose or high-dose, did not affect the spontaneous firing of Chls in the slice, arguing that the effects of AMPH on Chl activity, measured with p-rpS6<sup>240/244</sup> at 24h<sub>pi</sub>, involve extrinsic synaptic input to the Str.

### Single dose of AMPH affects Chl activity

P-rpS6<sup>240/244</sup> signal reports the integrated activity and p-rpS6<sup>240/244</sup> intensity changes appear to be detected 60 min after pharmacological or behavioral manipulations (Bertran-Gonzalez et al., 2012), suggesting that p-rpS6<sup>240/244</sup> is suitable to study Chl activity at 2.5h<sub>pi</sub> or later (Knight et al., 2012). Therefore, the lack of AMPH effect at 2.5h<sub>pi</sub> is not because of temporal limits of p-rpS6<sup>240/244</sup> measurement. Stress increases p-rpS6<sup>240/244</sup> intensity (Knight et al., 2012; Biever et al., 2015a), this may be reflected in the greater p-rpS6<sup>240/244</sup> intensity in the 2.5h<sub>pi</sub> compared with the 24h<sub>pi</sub> saline controls.

In the present study, p-rpS6<sup>240/244</sup> intensity in Chls was not affected at 2.5h<sub>pi</sub> after low-dose or high-dose AMPH, while Chl activity modulation via DA neuron glutamatergic

cotransmission is dose dependently attenuated after a single dose of AMPH 2.5h<sub>pi</sub> (Chuhma et al., 2014). This discrepancy could be because of differences in the measurements; p-rpS6<sup>240/244</sup> reflects the tonic *in vivo* activity of Chls, which also receive cortical and thalamic glutamatergic inputs in addition to DA neuron inputs (Lim et al., 2014), in contrast to the short phasic firing control of Chls by DA neuron synaptic inputs.

Psychostimulants, including cocaine, methamphetamine and AMPH, are associated with an overall downregulation of DA transmission, both DA release and D2 receptor levels (Ashok et al., 2017). So, we should have expected an increase in Chl activity because of the loss of D2 receptor inhibition. In contrast, the attenuation of Chl activity at 24h<sub>pi</sub> argues for polysynaptic effects extending beyond direct effects on DA neuron presynaptic terminals. Indeed, AMPH-induced DA release has an onset of minutes and lasts for about 1 h in rodents (Sulzer, 2011), in parallel with behavioral activation. Tonic attenuation of cortical or thalamic glutamatergic inputs may be caused by polysynaptic modulation, resulting in delayed attenuation of Chl activity. Since AMPH does not affect p-rpS6<sup>240/244</sup> levels or protein synthesis in the Str within 2 h following injection (Rapanelli et al., 2014; Biever et al., 2015b), 2.5 h does not appear to be sufficient to cause long-term circuit changes.

Polysynaptic mechanisms that could contribute to observed decreases in Chl activity in the ventral Str/NAc may involve AMPH effects on other neurotransmitters besides DA. Glutamate efflux in the ventral tegmental area (VTA) is affected by AMPH administration, although both an increase (Xue et al., 1996) and a decrease (Wolf and Xue, 1998) of glutamate efflux have been observed. Acute AMPH exposure induces attenuation of excitatory glutamatergic synaptic transmission in the VTA by activation of serotonin receptors (Jones and Kauer, 1999). AMPH also indirectly affects DA release by stimulating the trace amine-associated receptors (TAAR1) expressed in DA neuron presynaptic terminals (Underhill et al., 2021).

### Chls in psychostimulant-induced changes

In the present study, low-dose AMPH significantly attenuated Chl activity in the ventral Str/NAc, a crucial site of psychostimulant action (Russo et al., 2010; Sulzer, 2011). DA neurons projecting to the ventral Str/NAc that corelease glutamate (Hnasko et al., 2010; Stuber et al., 2010) can drive burst firing in Chls (Chuhma et al., 2014; Mingote et al., 2019). A single dose of AMPH attenuates glutamate cotransmission (Chuhma et al., 2014), and mice with conditional reduction in glutamate cotransmission show an attenuated sensitization to repeated AMPH (Mingote et al., 2017). Similarly, we found here that AMPH attenuated Chl activity at 24h<sub>pi</sub> only in the ventral Str/NAc, suggesting that DA neuron glutamate cotransmission may be one of the factors responsible for NAc-selective attenuation of Chls by low-dose AMPH, in addition to attenuation of phasic firing control through direct synaptic connections of DA neurons.

Although psychostimulant addiction involves repeated use, a single dose of AMPH can induce enduring Str

circuit changes, drug-dependent behavior and negative affective states, such as anhedonia, depression and anxiety (Vanderschuren et al., 1999; Koob and Le Moal, 2001; Xia et al., 2008; Kameda et al., 2011; Li et al., 2017; Jing et al., 2018; Rincón-Cortés et al., 2018; Jayanthi et al., 2020). Interestingly, even a single dose of AMPH has been found to induce behavioral and neurochemical sensitization, which appears to increase over weeks (Robinson, 1984; Vanderschuren et al., 1999). Our results, in line with these previous findings, point to the relevance of a single dose of AMPH for elucidating drug-induced plasticity. Enduring alterations in Ch1 activity following acute AMPH exposure point to Ch1s as a key component of drug-induced plasticity in the Str circuitry. Further studies using mice with restricted expression of opsins in ChAT neurons will be required to explore whether this reduction in NAc Ch1 activity is important in subsequent drug-dependent behavior.

## References

- Abudukeyoumu N, Hernandez-Flores T, Garcia-Munoz M, Arbutnott GW (2019) Cholinergic modulation of striatal microcircuits. *Eur J Neurosci* 49:604–622.
- Ashok AH, Mizuno Y, Volkow ND, Howes OD (2017) Association of stimulant use with dopaminergic alterations in users of cocaine, amphetamine, or methamphetamine: a systematic review and meta-analysis. *JAMA Psychiatry* 74:511–519.
- Atallah HE, McCool AD, Howe MW, Graybiel AM (2014) Neurons in the ventral striatum exhibit cell-type-specific representations of outcome during learning. *Neuron* 82:1145–1156.
- Bäckman CM, Malik N, Zhang Y, Shan L, Grinberg A, Hoffer BJ, Westphal H, Tomac AC (2006) Characterization of a mouse strain expressing Cre recombinase from the 3' untranslated region of the dopamine transporter locus. *Genesis* 44:383–390.
- Bertran-Gonzalez J, Chieng BC, Laurent V, Valjent E, Balleine BW (2012) Striatal cholinergic interneurons display activity-related phosphorylation of ribosomal protein S6. *PLoS One* 7:e53195.
- Biever A, Valjent E, Puighermanal E (2015a) Ribosomal protein S6 phosphorylation in the nervous system: from regulation to function. *Front Mol Neurosci* 8:75.
- Biever A, Puighermanal E, Nishi A, David A, Panciatici C, Longueville S, Xirodimas D, Gangarossa G, Meyuhas O, Hervé D, Girault JA, Valjent E (2015b) PKA-dependent phosphorylation of ribosomal protein S6 does not correlate with translation efficiency in striatonigral and striatopallidal medium-sized spiny neurons. *J Neurosci* 35:4113–4130.
- Brauer K, Häusser M, Hartig W, Arendt T (2000) The core-shell dichotomy of nucleus accumbens in the rhesus monkey as revealed by double-immunofluorescence and morphology of cholinergic interneurons. *Brain Res* 858:151–162.
- Chohan MO, Esses S, Haft J, Ahmari SE, Veenstra-VanderWeele J (2020) Altered baseline and amphetamine-mediated behavioral profiles in dopamine transporter Cre (DAT-IRES-Cre) mice compared to tyrosine hydroxylase Cre (TH-Cre) mice. *Psychopharmacology (Berl)* 237:3553–3568.
- Chuhma N, Mingote S, Moore H, Rayport S (2014) Dopamine neurons control striatal cholinergic neurons via regionally heterogeneous dopamine and glutamate signaling. *Neuron* 81:901–912.
- Chuhma N, Mingote S, Yetnikoff L, Kalmbach A, Ma T, Ztaou S, Sienna AC, Tepler S, Poulin JF, Ansorge M, Awatramani R, Kang UJ, Rayport S (2018) Dopamine neuron glutamate cotransmission evokes a delayed excitation in lateral dorsal striatal cholinergic interneurons. *Elife* 7:e39786.
- Cunningham J, McCrum-Gardner E (2007) Power, effect and sample size using GPower: practical issues for researchers and members of research ethics committees. *Evidence Based Midwifery* 5:132–136.
- Faul F, Erdfelder E, Lang AG, Buchner A (2007) G\*Power 3: a flexible statistical power analysis program for the social, behavioral, and biomedical sciences. *Behav Res Methods* 39:175–191.
- Gangarossa G, Valjent E (2012) Regulation of the ERK pathway in the dentate gyrus by in vivo dopamine D1 receptor stimulation requires glutamatergic transmission. *Neuropharmacology* 63:1107–1117.
- Gaytan O, Swann A, Dafny N (1998) Time-dependent differences in the rat's motor response to amphetamine. *Pharmacol Biochem Behav* 59:459–467.
- Goldberg JA, Wilson CJ (2010) The cholinergic interneurons of the striatum: intrinsic properties underlie multiple discharge patterns. *Hbk Behav Neurosci* 20:133–149.
- Gonzales KK, Smith Y (2015) Cholinergic interneurons in the dorsal and ventral striatum: anatomical and functional considerations in normal and diseased conditions. *Ann NY Acad Sci* 1349:1–45.
- Goodwin JS, Larson GA, Swant J, Sen N, Javitch JA, Zahniser NR, De Felice LJ, Khoshbouei H (2009) Amphetamine and methamphetamine differentially affect dopamine transporters in vitro and in vivo. *J Biol Chem* 284:2978–2989.
- Granado N, Ares-Santos S, Tizabi Y, Moratalla R (2018) Striatal reinnervation process after acute methamphetamine-induced dopaminergic degeneration in mice. *Neurotox Res* 34:627–639.
- Hnasko TS, Chuhma N, Zhang H, Goh GY, Sulzer D, Palmiter RD, Rayport S, Edwards RH (2010) Vesicular glutamate transport promotes dopamine storage and glutamate corelease in vivo. *Neuron* 65:643–656.
- Holt DJ, Hersh LB, Saper CB (1996) Cholinergic innervation in the human striatum: a three-compartment model. *Neuroscience* 74:67–87.
- Jayanthi S, Torres OV, Ladenheim B, Cadet JL (2020) A single prior injection of methamphetamine enhances methamphetamine self-administration (SA) and blocks SA-induced changes in DNA methylation and mRNA expression of potassium channels in the rat nucleus accumbens. *Mol Neurobiol* 57:1459–1472.
- Jing L, Liu B, Zhang M, Liang JH (2018) Involvement of dopamine D2 receptor in a single methamphetamine-induced behavioral sensitization in C57BL/6J mice. *Neurosci Lett* 681:87–92.
- Jones S, Kauer JA (1999) Amphetamine depresses excitatory synaptic transmission via serotonin receptors in the ventral tegmental area. *J Neurosci* 19:9780–9787.
- Kalivas PW, Stewart J (1991) Dopamine transmission in the initiation and expression of drug- and stress-induced sensitization of motor activity. *Brain Res Brain Res Rev* 16:223–244.
- Kameda SR, Fukushima DF, Trombin TF, Procópio-Souza R, Patti CL, Hollais AW, Calzavara MB, Abílio VC, Ribeiro RA, Tufik S, D'Almeida V, Frussa-Filho R (2011) Adolescent mice are more vulnerable than adults to single injection-induced behavioral sensitization to amphetamine. *Pharmacol Biochem Behav* 98:320–324.
- Kelley AE (2001) Measurement of rodent stereotyped behavior. *Curr Protoc Neurosci Chapter 8:Unit 8.8*.
- Kharkwal G, Brami-Cherrier K, Lizardi-Ortiz JE, Nelson AB, Ramos M, Del Barrio D, Sulzer D, Kreitzer AC, Borrelli E (2016) Parkinsonism driven by antipsychotics originates from dopaminergic control of striatal cholinergic interneurons. *Neuron* 91:67–78.
- Knight ZA, Tan K, Birsoy K, Schmidt S, Garrison JL, Wysocki RW, Emiliano A, Ekstrand MI, Friedman JM (2012) Molecular profiling of activated neurons by phosphorylated ribosome capture. *Cell* 151:1126–1137.
- Koob GF, Le Moal M (2001) Drug addiction, dysregulation of reward, and allostasis. *Neuropsychopharmacology* 24:97–129.
- Krasnova IN, Ladenheim B, Jayanthi S, Oyler J, Moran TH, Huestis MA, Cadet JL (2001) Amphetamine-induced toxicity in dopamine terminals in CD-1 and C57BL/6J mice: complex roles for oxygen-based species and temperature regulation. *Neuroscience* 107:265–274.
- Krasnova IN, Ladenheim B, Cadet JL (2005) Amphetamine induces apoptosis of medium spiny striatal projection neurons via the mitochondria-dependent pathway. *FASEB J* 19:851–853.

- Lee JH, Ribeiro EA, Kim J, Ko B, Kronman H, Jeong YH, Kim JK, Janak PH, Nestler EJ, Koo JW, Kim JH (2020) Dopaminergic regulation of nucleus accumbens cholinergic interneurons demarcates susceptibility to cocaine addiction. *Biol Psychiatry* 88:746–757.
- Lewis RG, Borrelli E (2020) A mechanism of cocaine addiction susceptibility through D2 receptor-mediated regulation of nucleus accumbens cholinergic interneurons. *Biol Psychiatry* 88:738–740.
- Li MH, Underhill SM, Reed C, Phillips TJ, Amara SG, Ingram SL (2017) Amphetamine and methamphetamine increase NMDAR-GluN2B synaptic currents in midbrain dopamine neurons. *Neuropsychopharmacology* 42:1539–1547.
- Lim SA, Kang UJ, McGehee DS (2014) Striatal cholinergic interneuron regulation and circuit effects. *Front Synaptic Neurosci* 6:22.
- Matamales M, Götz J, Bertran-Gonzalez J (2016a) Quantitative imaging of cholinergic interneurons reveals a distinctive spatial organization and a functional gradient across the mouse striatum. *PLoS One* 11:e0157682.
- Matamales M, Skrbis Z, Hatch RJ, Balleine BW, Götz J, Bertran-Gonzalez J (2016b) Aging-related dysfunction of striatal cholinergic interneurons produces conflict in action selection. *Neuron* 90:362–373.
- Miller DB, O'Callaghan JP (1996) Neurotoxicity of d-amphetamine in the C57BL/6J and CD-1 mouse. Interactions with stress and the adrenal system. *Ann NY Acad Sci* 801:148–167.
- Mingote S, Chuhma N, Kusnoor SV, Field B, Deutch AY, Rayport S (2015) Functional connectome analysis of dopamine neuron glutamatergic connections in forebrain regions. *J Neurosci* 35:16259–16271.
- Mingote S, Chuhma N, Kalmbach A, Thomsen GM, Wang Y, Mihali A, Sferazza C, Zucker-Scharff I, Siena AC, Welch MG, Lizardi-Ortiz J, Sulzer D, Moore H, Gaisler-Salomon I, Rayport S (2017) Dopamine neuron dependent behaviors mediated by glutamate cotransmission. *Elife* 6:e27566.
- Mingote S, Amsellem A, Kempf A, Rayport S, Chuhma N (2019) Dopamine-glutamate neuron projections to the nucleus accumbens medial shell and behavioral switching. *Neurochem Int* 129:104482.
- Paxinos G, Franklin KBJ (2008) The mouse brain in stereotaxic coordinates, Ed 3. San Diego:Elsevier/Academic Press.
- Phelps PE, Vaughn JE (1986) Immunocytochemical localization of choline acetyltransferase in rat ventral striatum: a light and electron microscopic study. *J Neurocytol* 15:595–617.
- Rapanelli M, Frick LR, Pogorelov V, Ota KT, Abbasi E, Ohtsu H, Pittenger C (2014) Dysregulated intracellular signaling in the striatum in a pathophysiologically grounded model of Tourette syndrome. *Eur Neuropsychopharmacol* 24:1896–1906.
- Ricaurte GA, Seiden LS, Schuster CR (1984) Further evidence that amphetamines produce long-lasting dopamine neurochemical deficits by destroying dopamine nerve fibers. *Brain Res* 303:359–364.
- Rincón-Cortés M, Gagnon KG, Dollish HK, Grace AA (2018) Diazepam reverses increased anxiety-like behavior, social behavior deficit, and dopamine dysregulation following withdrawal from acute amphetamine. *Neuropsychopharmacology* 43:2418–2425.
- Robinson TE (1984) Behavioral sensitization: characterization of enduring changes in rotational behavior produced by intermittent injections of amphetamine in male and female rats. *Psychopharmacology (Berl)* 84:466–475.
- Robinson TE, Becker JB (1986) Enduring changes in brain and behavior produced by chronic amphetamine administration: a review and evaluation of animal models of amphetamine psychosis. *Brain Res* 396:157–198.
- Russo SJ, Dietz DM, Dumitriu D, Morrison JH, Malenka RC, Nestler EJ (2010) The addicted synapse: mechanisms of synaptic and structural plasticity in nucleus accumbens. *Trends Neurosci* 33:267–276.
- Ryan LJ, Linder JC, Martone ME, Groves PM (1990) Histological and ultrastructural evidence that D-amphetamine causes degeneration in neostriatum and frontal cortex of rats. *Brain Res* 518:67–77.
- Sofuoglu M, Mooney M (2009) Cholinergic functioning in stimulant addiction: implications for medications development. *CNS Drugs* 23:939–952.
- Stuber GD, Hnasko TS, Britt JP, Edwards RH, Bonci A (2010) Dopaminergic terminals in the nucleus accumbens but not the dorsal striatum corelease glutamate. *J Neurosci* 30:8229–8233.
- Sulzer D (2011) How addictive drugs disrupt presynaptic dopamine neurotransmission. *Neuron* 69:628–649.
- Underhill SM, Hullihen PD, Chen J, Fenollar-Ferrer C, Rizzo MA, Ingram SL, Amara SG (2021) Amphetamines signal through intracellular TAAR1 receptors coupled to  $G_{\alpha_{13}}$  and  $G_{\alpha_S}$  in discrete subcellular domains. *Mol Psychiatry* 26:1208–1223.
- Valjent E, Bertran-Gonzalez J, Bowling H, Lopez S, Santini E, Matamales M, Bonito-Oliva A, Hervé D, Hoeffler C, Klann E, Girault JA, Fisone G (2011) Haloperidol regulates the state of phosphorylation of ribosomal protein S6 via activation of PKA and phosphorylation of DARPP-32. *Neuropsychopharmacology* 36:2561–2570.
- Vanderschuren LJ, Schmidt ED, De Vries TJ, Van Moorsel CA, Tilders FJ, Schoffelmeer AN (1999) A single exposure to amphetamine is sufficient to induce long-term behavioral, neuroendocrine, and neurochemical sensitization in rats. *J Neurosci* 19:9579–9586.
- Wagner GC, Ricaurte GA, Johanson CE, Schuster CR, Seiden LS (1980) Amphetamine induces depletion of dopamine and loss of dopamine uptake sites in caudate. *Neurology* 30:547–550.
- Witten IB, Lin SC, Brodsky M, Prakash R, Diester I, Anikeeva P, Gradinaru V, Ramakrishnan C, Deisseroth K (2010) Cholinergic interneurons control local circuit activity and cocaine conditioning. *Science* 330:1677–1681.
- Wolf ME, Xue CJ (1998) Amphetamine and D1 dopamine receptor agonists produce biphasic effects on glutamate efflux in rat ventral tegmental area: modification by repeated amphetamine administration. *J Neurochem* 70:198–209.
- Xia YF, He L, Whistler JL, Hjelmstad GO (2008) Acute amphetamine exposure selectively desensitizes kappa-opioid receptors in the nucleus accumbens. *Neuropsychopharmacology* 33:892–900.
- Xue CJ, Ng JP, Li Y, Wolf ME (1996) Acute and repeated systemic amphetamine administration: effects on extracellular glutamate, aspartate, and serine levels in rat ventral tegmental area and nucleus accumbens. *J Neurochem* 67:352–363.
- Yates JW, Meij JT, Sullivan JR, Richtand NM, Yu L (2007) Bimodal effect of amphetamine on motor behaviors in C57BL/6 mice. *Neurosci Lett* 427:66–70.
- Zhu JP, Xu W, Angulo JA (2006) Methamphetamine-induced cell death: selective vulnerability in neuronal subpopulations of the striatum in mice. *Neuroscience* 140:607–622.